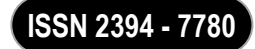
# **International Journal of Advance and Innovative Research**

Volume 12, Issue 3: July - September 2025



# RECYCLING ALLOY WASTE INTO Fe<sub>2</sub>O<sub>3</sub>@g-C<sub>3</sub>N<sub>4</sub> NANOCOMPOSITE: A SUSTAINABLE PATHWAY FOR ENVIRONMENTAL REMEDIATION

## Mr. Aman. Patel

The Cathedral and John Connon Senior School, Mumbai – 400001

## **ABSTRACT**

The recycling of industrial waste into functional nanomaterials offers a sustainable route to address both environmental pollution and resource utilization. In this study, Ni–Fe alloy waste was repurposed as a precursor for the synthesis of  $Fe_2O_3$  nanoparticles via an acid leaching–calcination route. The obtained  $Fe_2O_3$  nanoparticles were subsequently integrated with graphitic carbon nitride  $(g-C_3N_4)$  through a simple calcination process to fabricate  $Fe_2O_3@g-C_3N_4$  composites. Structural and morphological analyses confirmed the successful anchoring of  $Fe_2O_3$  nanoparticles onto  $g-C_3N_4$  sheets, establishing strong interfacial interactions between the two components. The photocatalytic activity of the composites was evaluated using methyl orange (MO) dye as a model pollutant under visible light irradiation. While pristine  $g-C_3N_4$  and  $Fe_2O_3$  nanoparticles achieved 31.84% and 65.01% degradation within 120 min, respectively, the  $Fe_2O_3@g-C_3N_4$  composite exhibited superior performance with 92.68% degradation in the same duration. The enhanced efficiency is attributed to improved charge separation, synergistic heterojunction effects, and the increased surface-active sites provided by the composite structure. This work demonstrates the potential of recycling Ni–Fe alloy waste into high-performance photocatalysts, aligning with circular economy principles and offering a sustainable solution for wastewater remediation.

**Keywords:** Fe<sub>2</sub>O<sub>3</sub> nanoparticles, waste recycling, dye degradation.

## INTRODUCTION

The widespread generation of electronic waste (e-waste) has emerged as a significant environmental challenge in recent decades. With the rapid pace of technological advancement and shortened product life cycles, discarded electronic devices and components are accumulating at an alarming rate. These materials often contain a variety of valuable yet potentially hazardous metals such as iron, nickel, copper, and rare earth elements. Improper disposal of e-waste not only leads to resource depletion but also poses serious environmental and health risks due to leaching of toxic metals into soil and water systems. Recycling and repurposing valuable metals from e-waste offer a sustainable solution, enabling resource recovery while minimizing environmental impact. In particular, using metal-rich waste streams as precursors for advanced functional materials provides a compelling strategy for addressing both pollution and material scarcity. Against this backdrop, semiconductor photocatalysis has gained attention as a green technology for environmental remediation—especially for the degradation of persistent organic pollutants such as synthetic dyes in industrial wastewater. (Chen et al., 2024; Far et al., 2022; Li et al., 2020)

The uncontrolled discharge of dye-containing effluents into aquatic environments has become an escalating global concern due to their persistence, toxicity, and detrimental impacts on ecosystems and human health. Synthetic dyes, commonly used in textile, paper, and dyeing industries, often resist conventional wastewater treatment owing to their stable aromatic structures and low biodegradability. The development of efficient, cost-effective, and environmentally friendly technologies for dye degradation is therefore a critical priority. Among emerging solutions, semiconductor photocatalysis has attracted considerable attention as a promising approach for the complete mineralization of recalcitrant organic pollutants under visible-light irradiation.

Graphitic carbon nitride  $(g-C_3N_4)$  has emerged as a promising visible-light-responsive photocatalyst due to its suitable bandgap (~2.7 eV), low cost, environmental stability, and facile synthesis from nitrogen-rich precursors like melamine or urea. However, its practical application is limited by factors such as rapid recombination of photogenerated electron—hole pairs, a relatively low specific surface area, and suboptimal absorption in the visible-light spectrum. To overcome these challenges, researchers have explored various modification strategies including morphological tuning, surface functionalization, and the incorporation of metal or metal oxide species to enhance charge carrier dynamics and photocatalytic efficiency. (Weldekirstos et al., 2024)

Iron oxide (Fe<sub>2</sub>O<sub>3</sub>) is a widely studied cocatalyst that offers excellent redox activity, visible-light absorption, and the potential to facilitate charge separation when coupled with g-C<sub>3</sub>N<sub>4</sub>. The formation of a heterojunction between g-C<sub>3</sub>N<sub>4</sub> and Fe<sub>2</sub>O<sub>3</sub> can significantly enhance photocatalytic activity by promoting efficient electron transfer and suppressing recombination losses. Moreover, the use of waste-derived iron as a dopant source not only reduces synthesis costs but also supports circular economy principles by repurposing industrial residues into high-value environmental materials. (Wei et al., 2024; Zhou et al., 2016)

# **International Journal of Advance and Innovative Research**

Volume 12, Issue 3: July - September 2025

ISSN 2394 - 7780

In this study, waste Ni–Fe alloy—commonly found in machining and metallurgical industries and present in some forms of e-waste—was employed as a recyclable iron source for the fabrication of Fe<sub>2</sub>O<sub>3</sub>@g-C<sub>3</sub>N<sub>4</sub> photocatalysts. Iron was selectively leached from the alloy using sulfuric acid (H<sub>2</sub>SO<sub>4</sub>) under controlled conditions, producing an iron-rich solution that served as the precursor for Fe<sub>2</sub>O<sub>3</sub> formation. While the alloy contained both nickel and iron, only iron was incorporated into the final composite, allowing for targeted utilization of the metal relevant for photocatalytic performance. This process not only diverts waste from landfill but also enables sustainable synthesis of active photocatalytic materials.

The resulting  $Fe_2O_3@g-C_3N_4$  composite is anticipated to demonstrate enhanced photocatalytic performance due to several synergistic effects: (i) expanded visible-light absorption, (ii) effective suppression of charge carrier recombination, and (iii) increased density of active sites due to  $Fe_2O_3$  incorporation. Photocatalytic experiments using model dye pollutants were conducted under visible-light irradiation to evaluate and compare the activity of the composite against pristine  $g-C_3N_4$ .

To confirm the successful synthesis and understand structural and morphological features, the materials were characterized using X-ray diffraction (XRD), Fourier-transform infrared spectroscopy (FTIR), and scanning electron microscopy (SEM). XRD was used to identify the crystalline phases and confirm Fe<sub>2</sub>O<sub>3</sub> formation; FTIR helped analyze chemical bonding and functional groups; and SEM revealed the surface morphology and distribution of Fe<sub>2</sub>O<sub>3</sub> on g-C<sub>3</sub>N<sub>4</sub>.

Overall, this work highlights the dual benefits of e-waste recycling and enhanced photocatalysis by transforming Ni–Fe alloy waste into a functional Fe<sub>2</sub>O<sub>3</sub>@g-C<sub>3</sub>N<sub>4</sub> composite. The study supports the development of cost-effective, sustainable materials for wastewater treatment while addressing critical environmental concerns associated with metal-rich waste disposal.

## 2. EXPERIMENTAL SECTION

## 2.1 Materials

Ni-Fe alloy waste was collected from a local machining industry. Melamine (99%) Sigma Aldrich, Hydrochloric acid (37%) Sigma Aldrich, Ethanol (99.5%) Sigma Aldrich and Methyl orange (90%). All solutions were prepared with distilled water.

## 2.2 Preparation of g-C<sub>3</sub>N<sub>4</sub>

g-C<sub>3</sub>N<sub>4</sub> sheets were synthesized by thermal co-polymerization of melamine and urea in a 7:3 weight ratio. Specifically, 7 g of melamine and 3 g of urea were thoroughly mixed in a mortar to obtain a uniform blend. The mixed powder was transferred into a covered alumina crucible to minimize sublimation losses during heating. The crucible was placed in a muffle furnace and heated to 550 °C at a ramp rate of 5 °C/min. The temperature was maintained at 550 °C for 3 hours to complete the polymerization and condensation reactions. During this process, urea decomposition produced gases that facilitated the formation of loosely stacked, sheet-like g-C<sub>3</sub>N<sub>4</sub> structures with increased surface area. After natural cooling to room temperature, the light-yellow product was collected, gently ground into a fine powder, and stored in airtight containers for further use.

## 2.3 Iron Leaching from Ni-Fe Alloy Waste

The Ni–Fe alloy waste was first cleaned by immersion in ethanol and briefly ultrasonicated to remove surface oils and loose debris. After drying at 60 °C, 2 g of the cleaned alloy was transferred into a 250 mL beaker. To leach iron, 30 mL of 5 M HCl solution was prepared by diluting concentrated hydrochloric acid in deionized water. The acid solution was carefully and slowly poured over the alloy with continuous gentle stirring at room temperature. Vigorous effervescence due to hydrogen gas evolution was observed, indicating active dissolution of iron. The reaction mixture was stirred for 1 hour to ensure effective leaching of iron into the solution. After completion of leaching, the suspension was filtered to remove undissolved solid residues (primarily nickel-rich or passivated particles). The resulting clear greenish filtrate, rich in Fe<sup>2+</sup> ions, was collected and evaporated to dryness. The dried residue was then calcined in a muffle furnace at 400 °C for 2 hours to obtain Fe<sub>2</sub>O<sub>3</sub> nanoparticles, which were subsequently used to dope onto g-C<sub>3</sub>N<sub>4</sub> for the synthesis of the Fe<sub>2</sub>O<sub>3</sub>@g-C<sub>3</sub>N<sub>4</sub> composite.

## 2.3 Synthesis of Fe<sub>2</sub>O<sub>3</sub>@g-C<sub>3</sub>N<sub>4</sub> Composite

The synthesized Fe<sub>2</sub>O<sub>3</sub> nanoparticles were then uniformly mixed with the g-C<sub>3</sub>N<sub>4</sub> powder by thorough grinding to ensure homogeneous distribution. The resulting mixture was transferred into a ceramic crucible and calcined at 400 °C for 2 hours to facilitate the anchoring of Fe<sub>2</sub>O<sub>3</sub> nanoparticles onto the g-C<sub>3</sub>N<sub>4</sub> sheets and improve structural integration. After cooling naturally to room temperature, the Fe<sub>2</sub>O<sub>3</sub>@g-C<sub>3</sub>N<sub>4</sub> composite was gently

ground into a fine powder and stored in airtight containers for further characterization and photocatalytic applications.

## 2.4 Characterization

The structural properties and phase composition of the synthesized materials were assessed using powder X-ray diffraction (XRD) on a Bruker AXS D8 Advance diffractometer. The morphology and microstructural characteristics were examined through Field Emission Scanning Electron Microscopy (FESEM) with an FEI Quanta 200F (Netherlands) equipped with a field emission gun (FEG). Additional surface morphology analysis was conducted using Scanning Electron Microscopy (SEM) on an FEI Quanta 200 (Netherlands), which utilizes a tungsten filament as the electron source. and UV-Vis spectroscopy on a Shimadzu UV-1800 spectrophotometer, within the 200–800 nm wavelength range at room temperature.

## 2.5 Photocatalytic Activity Evaluation

In this study, photodegradation experiments were carried out using a simulated solar light source with an intensity of 250 mW to evaluate the photocatalytic activity of the Fe<sub>2</sub>O<sub>3</sub>@g-C<sub>3</sub>N<sub>4</sub> composite in degrading methyl orange (MO) dye. 50 mg of the photocatalyst was dispersed in 100 mL of an aqueous solution containing 10 ppm of MO dye. The suspension was stirred in the dark for 30 minutes to establish adsorption—desorption equilibrium. During visible-light irradiation, 4 mL aliquots were withdrawn at predetermined time intervals, centrifuged to separate the photocatalyst, and analyzed by UV–Vis spectrophotometry. The residual MO concentration was determined by monitoring the absorbance at 464nm. All photocatalytic degradation tests were performed at room temperature under standard ambient conditions.

## **RESULTS AND DISCUSSION:**

The XRD pattern in Fig.1. confirms the successful incorporation of Fe<sub>2</sub>O<sub>3</sub> nanoparticles into the g-C<sub>3</sub>N<sub>4</sub> framework. For g-C<sub>3</sub>N<sub>4</sub>, two characteristic diffraction peaks are observed: a low-intensity peak at approximately 13.1° (002), corresponding to the in-plane structural packing of tri-s-triazine units, and a strong peak at approximately 27.3° (100), which is indexed to the interlayer stacking of conjugated aromatic systems (JCPDS 87-1526). In the Fe<sub>2</sub>O<sub>3</sub>@g-C<sub>3</sub>N<sub>4</sub> composite, both sets of peaks are present. The coexistence of the prominent g-C<sub>3</sub>N<sub>4</sub> (002) peak and the characteristic reflections of Fe<sub>2</sub>O<sub>3</sub> clearly demonstrates the successful formation of the heterostructure. A slight reduction in the intensity of the g-C<sub>3</sub>N<sub>4</sub> peak at 27.3° in the composite, along with peak broadening, indicates partial interaction between Fe<sub>2</sub>O<sub>3</sub> nanoparticles and the g-C<sub>3</sub>N<sub>4</sub> layers. This strong interfacial contact suggests efficient charge transfer pathways, which are advantageous for enhancing photocatalytic performance.(Christoforidis et al., 2016; Wang et al., 2022; Wei et al., 2024)

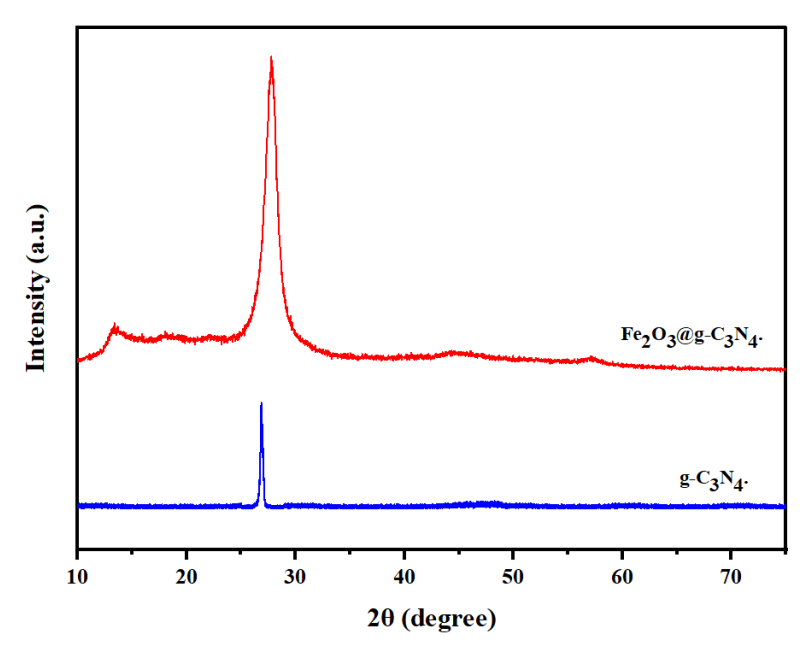


Fig.1. X-ray diffraction patterns of g-C<sub>3</sub>N<sub>4</sub> and Fe<sub>2</sub>O<sub>3</sub>@g-C<sub>3</sub>N<sub>4</sub> nanocomposite.

The FTIR spectrum in Fig.2. confirms the coexistence of functional groups belonging to both  $g-C_3N_4$  and  $Fe_2O_3$ . A strong absorption band at  $803~cm^{-1}$  corresponds to the bending vibration of the triazine ring, indicating the presence of the heptazine framework of  $g-C_3N_4$ . The multiple peaks observed at 1228, 1310, 1395, 1449, 1511, and  $1624~cm^{-1}$  are associated with the stretching vibrations of C-N and C=N bonds within the heterocyclic

Volume 12, Issue 3: July - September 2025

aromatic structure of g-C<sub>3</sub>N<sub>4</sub>. A broad band in the 3180–3160 cm<sup>-1</sup> region is attributed to N–H stretching vibrations and O–H groups arising from adsorbed water and residual surface functionalities. The distinct bands at 888 cm<sup>-1</sup> further support the presence of characteristic g-C<sub>3</sub>N<sub>4</sub> linkages. Importantly, the presence of Fe–O stretching vibrations below 600 cm<sup>-1</sup> validates the incorporation of Fe<sub>2</sub>O<sub>3</sub> nanoparticles within the g-C<sub>3</sub>N<sub>4</sub> matrix. The simultaneous appearance of Fe–O signals alongside g-C<sub>3</sub>N<sub>4</sub> vibrational modes, together with slight shifts in peak positions compared to pristine g-C<sub>3</sub>N<sub>4</sub>, indicates strong interfacial interactions between Fe<sub>2</sub>O<sub>3</sub> and g-C<sub>3</sub>N<sub>4</sub>. These interactions are expected to facilitate efficient charge transfer and improved photocatalytic activity of the composite.(Wang et al., 2022)

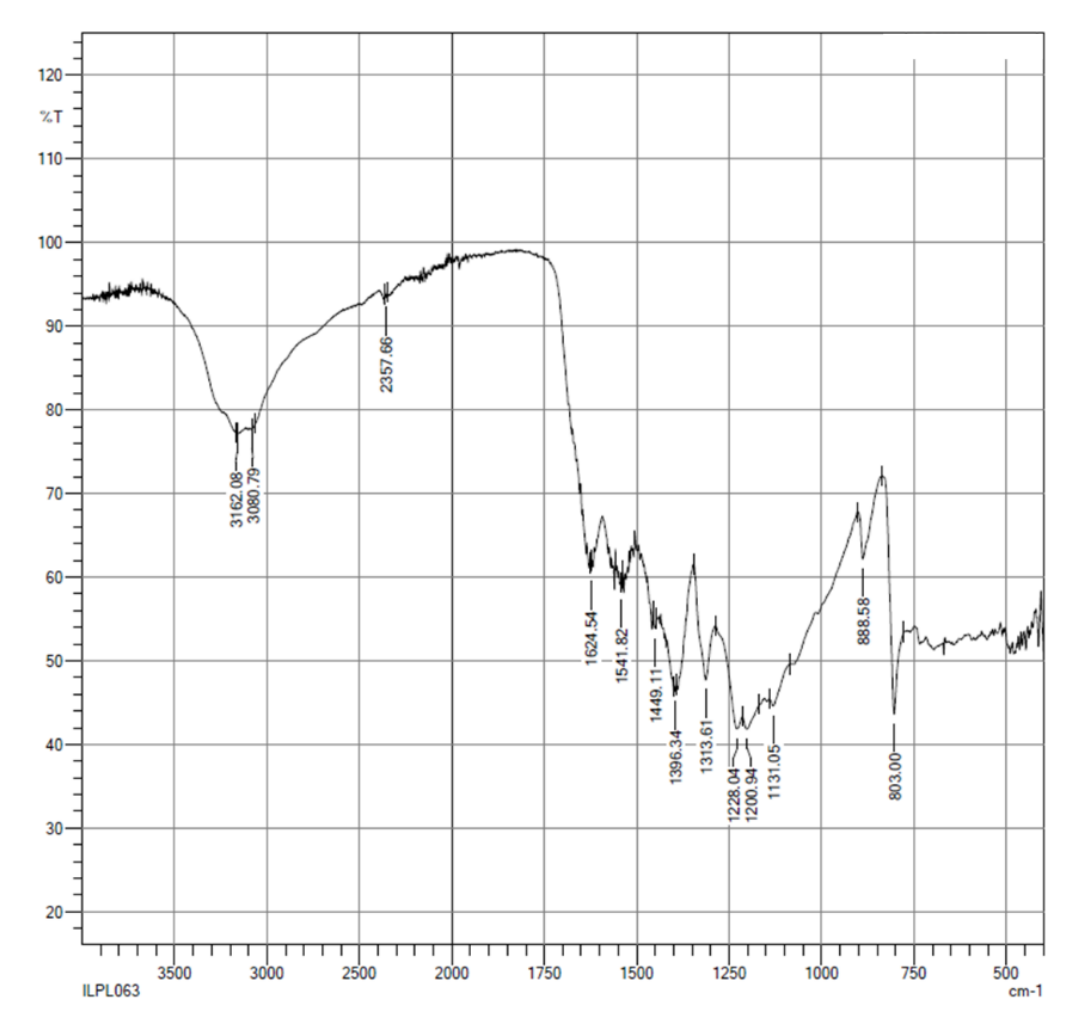


Fig.2. FTIR spectra of Fe<sub>2</sub>O<sub>3</sub>@g-C<sub>3</sub>N<sub>4</sub> nanocomposite.

The FESEM image in Fig.3. (a) depicts the characteristic morphology of pure g-C<sub>3</sub>N<sub>4</sub>, consisting of thin, stacked, and irregular nanosheets with a layered and wrinkled texture. These sheet-like structures are loosely arranged, generating a porous network with noticeable interlayer voids, which is a typical feature of g-C<sub>3</sub>N<sub>4</sub> obtained via thermal polymerization. The crumpled and rough surface morphology contributes to an increased specific surface area, thereby providing numerous active sites that facilitate photocatalytic reactions. As illustrated in Figure X, (b) the Fe<sub>2</sub>O<sub>3</sub> nanoparticles display a highly agglomerated, cluster-like morphology with rough and irregular surfaces. The particles exhibit nanoscale dimensions with noticeable aggregation due to strong interparticle interactions. (c) The g-C<sub>3</sub>N<sub>4</sub> framework illustrates relatively smooth, sheet-like regions, while the Fe<sub>2</sub>O<sub>3</sub> nanoparticles appear as densely packed clusters distributed across the g-C<sub>3</sub>N<sub>4</sub> surface. The nanoparticles are well-anchored onto the g-C<sub>3</sub>N<sub>4</sub> matrix, suggesting strong interfacial interaction between the two components. In contrast to previously reported morphologies featuring more discrete and uniformly dispersed particles, the present sample demonstrates pronounced aggregation and irregular surface textures, which are expected to enhance photocatalytic activity by providing abundant active sites. (Sumathi et al., 2019)

Volume 12, Issue 3: July - September 2025

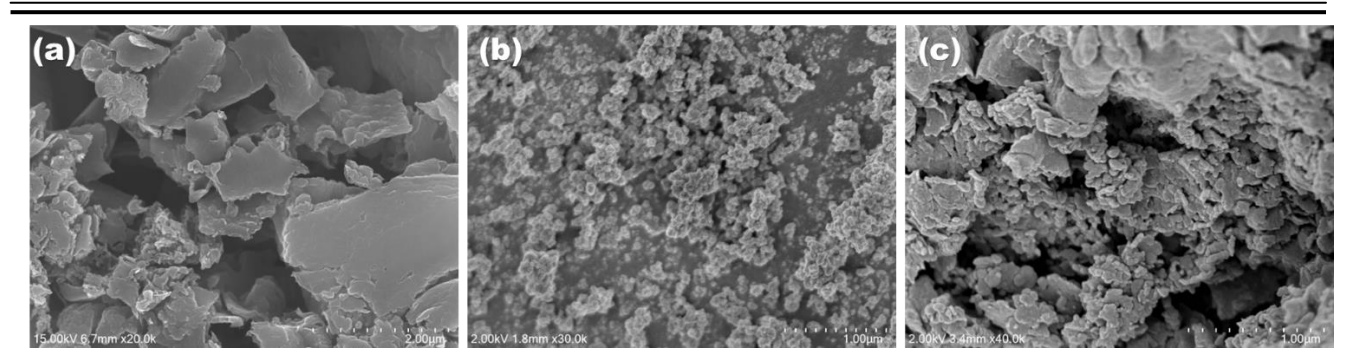


Fig.3. FESEM micrographs of (a) pristine g-C<sub>3</sub>N<sub>4</sub>, (b) Fe<sub>2</sub>O<sub>3</sub> nanoparticles and (c) Fe<sub>2</sub>O<sub>3</sub>@g-C<sub>3</sub>N<sub>4</sub> composite.

The evaluation of the photocatalytic MO dye degradation performances of pure  $g-C_3N_4$ ,  $Fe_2O_3$  and  $Fe_2O_3@g-C_3N_4$  composite was conducted by degrading a specific concentration of MO dye solution under visible light irradiation. In a standard procedure, the maximum absorption peak of MO dye at 464 nm was utilized to examine the catalytic degradation process of the dye. Fig.4. In contrast, pure  $g-C_3N_4$  and  $Fe_2O_3$  exhibited relatively low photocatalytic activity, with only 31.84% and 65.01% MO degradation respectively, after visible light irradiation for 120 minutes. The blank analysis was conducted in the absence of a catalyst to assess the stability of MO under illumination conditions.

The degradation efficiency was calculated using the equation:

Decolorization efficiency (%) = 
$$\left(\frac{c_0 - c}{c_0}\right) \times 100$$
 (1)

where C<sub>0</sub> and C are the initial and final absorbances of MO solutions, respectively.

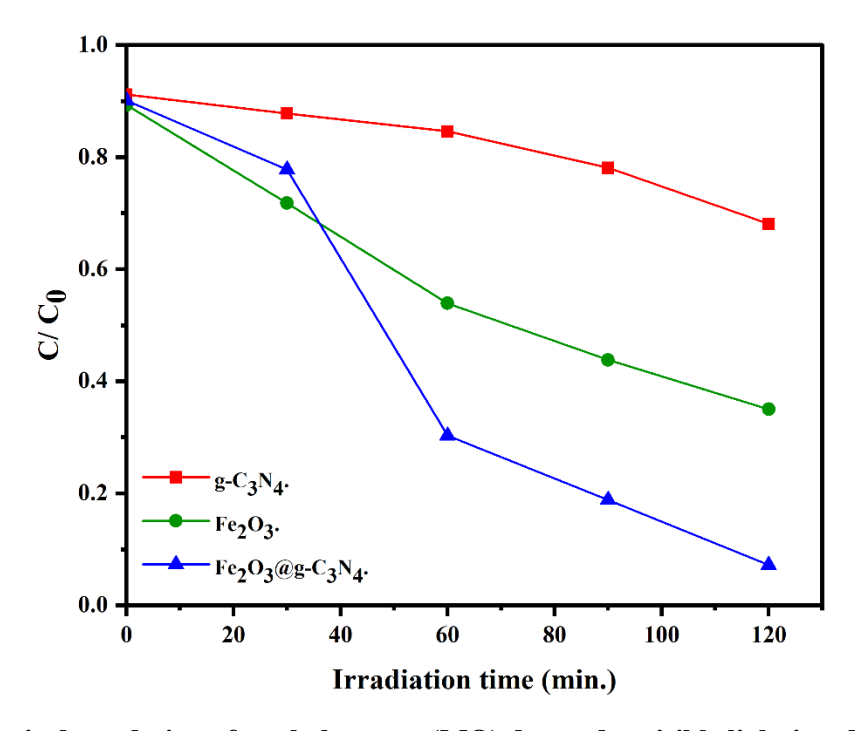


Fig.4. Photocatalytic degradation of methyl orange (MO) dye under visible light irradiation using g-C<sub>3</sub>N<sub>4</sub>, Fe<sub>2</sub>O<sub>3</sub>, and Fe<sub>2</sub>O<sub>3</sub>@g-C<sub>3</sub>N<sub>4</sub> photocatalysts.

## **CONCLUSION**

This work demonstrates a sustainable approach to waste recycling by repurposing expired iron syrup as a precursor for the synthesis of Fe<sub>2</sub>O<sub>3</sub> nanoparticles, which were further integrated with g-C<sub>3</sub>N<sub>4</sub> to form a Fe<sub>2</sub>O<sub>3</sub>@g-C<sub>3</sub>N<sub>4</sub> nanocomposite photocatalyst. FTIR analysis confirmed the presence of both Fe–O and g-C<sub>3</sub>N<sub>4</sub> characteristic peaks, with slight peak shifts indicating strong interfacial interactions. XRD patterns revealed the crystalline structure of Fe<sub>2</sub>O<sub>3</sub> embedded within the g-C<sub>3</sub>N<sub>4</sub> matrix, confirming successful composite formation. FESEM images showed a sheet-like morphology of g-C<sub>3</sub>N<sub>4</sub> with Fe<sub>2</sub>O<sub>3</sub> nanoparticles uniformly distributed across the surface, providing enhanced roughness and porosity favorable for photocatalysis.

# **International Journal of Advance and Innovative Research**

Volume 12, Issue 3: July - September 2025



Photocatalytic degradation studies using methyl orange (MO) dye under visible light revealed that pure g-C<sub>3</sub>N<sub>4</sub> achieved only 31.84% degradation in 120 min, while Fe<sub>2</sub>O<sub>3</sub> alone reached 65.01%. Notably, Fe<sub>2</sub>O<sub>3</sub>@g-C<sub>3</sub>N<sub>4</sub> exhibited superior performance with 92.68% degradation within the same period. The enhanced efficiency can be attributed to improved charge separation, stronger light harvesting, and a larger number of active sites resulting from the synergistic effect of Fe<sub>2</sub>O<sub>3</sub> and g-C<sub>3</sub>N<sub>4</sub>. Thus, this study not only validates the feasibility of recycling pharmaceutical waste into functional nanomaterials but also establishes Fe<sub>2</sub>O<sub>3</sub>@g-C<sub>3</sub>N<sub>4</sub> as a highly efficient and stable photocatalyst for environmental remediation.

## REFERENCES

- 1. Chen, M., Sun, M., Cao, X., Wang, H., Xia, L., Jiang, W., Huang, M., He, L., Zhao, X., & Zhou, Y. (2024). Progress in preparation, identification and photocatalytic application of defective g-C3N4. In *Coordination Chemistry Reviews* (Vol. 510). Elsevier B.V. https://doi.org/10.1016/j.ccr.2024.215849
- 2. Christoforidis, K. C., Montini, T., Bontempi, E., Zafeiratos, S., Jaén, J. J. D., & Fornasiero, P. (2016). Synthesis and photocatalytic application of visible-light active β-Fe2O3/g-C3N4 hybrid nanocomposites. *Applied Catalysis B: Environmental*, 187, 171–180. https://doi.org/10.1016/j.apcatb.2016.01.013
- 3. Far, H., Hamici, M., Brihi, N., Haddadi, K., Boudissa, M., Chihi, T., & Fatmi, M. (2022). High-performance photocatalytic degradation of NiO nanoparticles embedded on α-Fe2O3nanoporous layers under visible light irradiation. *Journal of Materials Research and Technology*, *19*, 1944–1960. https://doi.org/10.1016/j.jmrt.2022.05.159
- 4. Li, Y., Zhou, M., Cheng, B., & Shao, Y. (2020). Recent advances in g-C3N4-based heterojunction photocatalysts. In *Journal of Materials Science and Technology* (Vol. 56, pp. 1–17). Chinese Society of Metals. https://doi.org/10.1016/j.jmst.2020.04.028
- Sumathi, M., Prakasam, A., & Anbarasan, P. M. (2019). A facile microwave stimulated g-C3N4/α-Fe2O3 hybrid photocatalyst with superior photocatalytic activity and attractive cycling stability. *Journal of Materials Science: Materials in Electronics*, 30(12), 10985–10993. https://doi.org/10.1007/s10854-019-01439-1
- 6. Wang, W., Zhang, H., Chen, Y., & Shi, H. (2022). Efficient Degradation of Tetracycline via Coupling of Photocatalysis and Photo-Fenton Processes over a 2D/2D α-Fe2O3/g-C3N4 S-Scheme Heterojunction Catalyst. *Wuli Huaxue Xuebao/ Acta Physico Chimica Sinica*, 38(7). https://doi.org/10.3866/PKU.WHXB202201008
- 7. Wei, L., Zhang, X., Wang, J., Yang, J., & Yang, X. (2024). Synthesis of Fe2O3/g-C3N4 composite with efficient photocatalytic degradation for methyl orange. *Inorganic Chemistry Communications*, 159. https://doi.org/10.1016/j.inoche.2023.111890
- 8. Weldekirstos, H. D., Mengist, T., Belachew, N., & Mekonnen, M. L. (2024). Enhanced photocatalytic degradation of methylene blue dye using fascily synthesized g-C3N4/CoFe2O4 composite under sun light irradiation. *Results in Chemistry*, 7. https://doi.org/10.1016/j.rechem.2024.101306
- 9. Zhou, L., Wang, L., Zhang, J., Lei, J., & Liu, Y. (2016). Well-Dispersed Fe2O3Nanoparticles on g-C3N4for Efficient and Stable Photo-Fenton Photocatalysis under Visible-Light Irradiation. *European Journal of Inorganic Chemistry*, 2016(34), 5387–5392. https://doi.org/10.1002/ejic.201600959